Received: 17 November 2020 | Revised: 16 May 2021 | Accepted: 7 June 2021

IET Signal Processing

DOI: 10.1049/sil2.12064

The Institution of Engineering and Technology WILEY

ORIGINAL RESEARCH PAPER

A no-reference blurred colourful image quality assessment method based on dual maximum local information

Jian Chen | Shiyun Li | Li Lin

School of Electronic, Electrical Engineering and Physics, Fujian University of Technology, Fuzhou, Fujian, China

Correspondence

Jian Chen, School of Electronic, Electrical Engineering and Physics, Fujian University of Technology, Fuzhou, 350118, Fujian, China.
Email: jianchen@fjut.edu.cn

Funding information

Open Fund Project of Fujian Provincial Key Laboratory of Information Processing and Intelligent Control (Minjiang University), Grant/Award Number: MJUKF-IPIC202110; Natural Science Foundation of Fujian Province, Grant/Award Number: 2018J01637; Natural Science Foundation of Shanghai, Grant/Award Number: 19ZR1407200

Abstract

Images can be blurred due to the imperfection of the imaging system and blurriness is one of the challenging problems for image quality assessment (IQA). No-reference blurred IQA methods have been proposed in the literature to calculate image blurriness. Inspired by image processing-based auto-focussing and maximum local information theories, a no-reference blurred colourful IQA method based on Dual Maximum Local Information is proposed here. First, a window extraction method that combines the maximum gradient with local entropy is proposed to obtain the region of interest (ROI) for subsequent processing. Second, an improved maximum gradient method that leverages information from different channel images is presented to calculate the maximum gradient variation within the ROI for final sharpness score. Experimental results illustrated that the proposed method has better performance under various measurements compared with the state-of-the-art methods on LIVE, CSIQ, TID2008, TID2013, VCL@FER, IVC image databases.

1 | INTRODUCTION

Blurriness is one of the most common image distortion types in practice, which is introduced by the imperfection of the imaging systems. Consequently, image quality assessment (IQA) methods are highly required to evaluate the quality of blurred images. According to the available amount of reference information, IQA methods can be categorised into three classes: (1) full-reference image quality assessment (FR-IQA), (2) reduced-reference image quality assessment (RR-IQA) and (3) no-reference image quality assessment (NR-IQA) [1, 2]. For FR-IQA and RR-IQA methods, reference information such as an original high-quality image and some features from the original image that are usually not accessible in practice is needed. Therefore, NR-IQA methods are more useful for practical applications [3]. NR-IQA is also named as blind image quality assessment (BIQA), which can be categorised into learning-free and learning-based methods. Learning-free methods can be further classified into two categories: spatial domain and spectral domain methods, respectively.

In spatial domain, some methods are based on edge information in which gradient operators are commonly used. For example, Marziliano et al. [4] proposed to measure the spread of the edge via Sobel operator. In addition, a no-reference image sharpness method called the 'Just Noticeable Blur' (JNB) based on measuring the minimum amount of perceived blurriness around the edge was proposed [5]. Later, a method based on the cumulative probability of blur detection (CPBD) was proposed [6]. Feichtenhofer et al. [7] took human visual system into account and presented perceptual sharpness index (PSI) based on a statistical analysis of local edge gradients. Although previous methods own low computational complexity, the evaluation results are not reasonable when sharp edge is lacking. Therefore, some methods were proposed based on Tchebichef moment, which obtained better results [8, 9]. Based on the observation that human beings have difficulty in perceiving differences between a blurred image and the same re-blurred image, Crete et al. [10] proposed a method in which the blurriness was evaluated by comparison between intensity variations of neighbouring pixels of an input image before and

after applying a low-pass filter. Based on analysing the mathematical knowledge of Gaussian convolution, Bong et al. [11] proposed a method that also made use of the re-blurred image. Zhang et al. [12] proposed a no-reference structural similarity (NSSIM) metric based on re-blur theory and structural similarity index (SSIM) [13]. The methods based on re-blur theory own lower computational complexity. But as most methods integrated re-blur theory and different FR-IQA theories, evaluation results are easily affected by the introduced FR-IQA algorithms. There are also methods based on Free energy [14, 15].

In spectral domain, most methods are based on Discrete Fourier Transform (DFT), Discrete Cosine Transform (DCT) and Wavelet Transform (WT). To make use of more features, Vu et al. [16] utilised both spectral and spatial properties in which DFT was used. Caviedes et al. [17] proposed to calculate kurtosis of the DCT after detecting and enclosing edge pixels with blocks. Zhang et al. [18] presented a method based on the scale-invariant feature transform (SIFT) [19] and the sum of squared AC coefficients of DCT. Some methods based on WT are also presented [20–23]. More recently, Hosseini et al. [24] proposed a method that employed human vision system-like filter. Compared with the methods in the spatial domain, the methods in spectral domain own higher computational complexity. Meanwhile, as methods both in spatial domain and spectral domain simply use weight and normalisation to obtain the final evaluation scores after extracting different image features, the evaluation results are commonly not optimal.

To optimise the weight, several machine learning-based methods adopted support vector machine (SVM) to get better results. Those methods include some methods for general purpose and can be sorted into two categories [25–29]: overall framework and two-step framework. Methods from the former category predict NR-IQA results without distinguishing distortion types beforehand. Classical methods include BLIINDS-II [26] and BRISQUE [27]. On the other hand, methods from the latter category involve distortion identification followed by distortion-specific NR-IQA metric calculation. Classical methods include BIQI [28] and DIIVINE [29]. Recently, Cai et al. [30] leveraged the discrepancy measures of structural degradation in both the spatial and wavelet domains, and used a support vector regressor (SVR) to map the feature vectors into quality scores. Liu et al. [31] proposed a method that integrated an orientation-aware local pattern operator which fully considered the impact of anisotropy of orientation selectivity mechanism and the gradient orientation effect on visual perception. Although the methods based on machine learning get better results in general, the performance is determined by the introduced features. In recent years, deep learning-based NR-IQA methods for blurred images have received widespread attention. Compared with the SVM-based methods, deep learning-based methods could combine feature extraction and quality prediction together. For instance, Kang et al. [32] developed a Convolutional Neural Network (CNN) for NR-IQA, which combined feature learning and regression as a complete optimisation process. Bianco et al. [33] analysed the use of deep learning for distortion-generic NR-IQA; three steps were included are given as follows: image description using pre-trained CNNs, feature and prediction pooling strategies and fine-tunning of the CNN. Ma et al. [34] proposed a multi-task end-to-end optimised network (MEON) for BIQA, which consisted of two subtasks: the classification of distortion types and the prediction of the perceptual quality. Yan et al. [35] integrated natural scene statistics (NSS) features prediction task with the deep learning-based image quality prediction task that improved the representation ability and generalisation ability. Yang et al. [36] proposed an end-to-end saliency-guided deep neural network (SGDNet) in which two sub-tasks including visual saliency prediction and image quality prediction were jointly optimised with a shared feature extractor. He et al. [37] proposed a deep model which considered both the spatial and visual features of the testing image. Compared with machine learning-based methods, deep learning-based methods can achieve better evaluation results, but require more data for training.

Compared with the learning-based methods, methods in spatial/spectral domain are training-free, and therefore own better content independence. We propose an NR-IQA method in spatial domain based on a two-step framework, which is named Dual Maximum Local Information (DMLI). Inspired by focussing window (or region) selection strategy in the auto-focussing method, we propose the first maximum local information strategy that calculates the maximum gradient and local entropy in sliding windows to extract one region of interest (ROI) in a colourful image for subsequent processing. Then, the second maximum local information strategy that calculates the maximum gradient and the variability of gradient from different channel images of the ROI is proposed to obtain the final score.

The main contributions of our work are summarised as follows:

1. We propose a two-step framework for NR-IQA in spatial domain, which is opinion-unaware and based on DMLI.
2. ROI extraction strategy is proposed based on maximum gradient and local entropy.
3. The proposed framework is universal to different maximum information-based methods.

The rest of this paper is organised as follows. In Section 2, we introduce related works for the proposed method. In Section 3, we describe the details of the proposed method. The experimental results are presented in Section 4, followed by discussions and conclusion in Section 5.

2 | RELATED WORKS

2.1 | Region selection algorithms

For image processing-based auto-focussing, region selection algorithm plays an important role in the whole procedure, which can improve the real-time performance and focussing accuracy. Traditional region selection algorithms include centre

region algorithm, multi-region algorithm, golden section algorithm, which are all fixed region in an image [38]. Inevitably, background which appears smooth occupies some parts of the image in most cases. As a result, there are also some automatic region selection algorithms, which focussed on the region with more information. Wang et al. [39] proposed a region selection algorithm based on improved particle swarm optimisation (PSO) approach. Jeon et al. [40] proposed an entropy-based region selection algorithm. Liang et al. [41] and Lee et al. [42] also proposed different automatic algorithms for region selection in auto-focussing.

For NR-IQA methods in the spatial domain, edge area is more helpful compared with smooth area. Consequently, we can focus on the region with more edge information and exclude regions with higher smoothness. As illustrated in Figure 1, when we excluded the smooth regions in the image (shown in Figure 1c), the number of redundant pixel decreases (shown in rectangle of Figure 1b and d), which represents that the rest of image contains most of the edge area and is helpful for IQA calculation.

2.2 | NR-IQA methods based on maximum information

As image blurriness can be indicated by intensity variations in the pixel, a better indicator of blurriness can be obtained by employing the high variations in the pixel than low variations; Bahrami et al. [44] proposed a metric named maximum local variation (MLV), which represents the maximum intensity variation of the pixel with respect to its 8-neighbours. Similarly, Zhan et al. [45] leveraged the maximum gradient, which represents the sharpest spot in an image, as well as the variability of gradients, which represents variations within the content of the image. These methods are similar to edge information-based methods which use gradient information, but leverage the maximum variation/gradient of the pixel. Compared with Sobel operator-based methods, the methods based on maximum information own better evaluation performance.

Although those methods achieve competitive results, they just used the greyscale version of colourful images from different databases. A colourful image consists of three different channels; some information would be neglected if a colourful image is directly transformed into the corresponding greyscale image. To get a better insight of the differences between a colourful image and the corresponding greyscale image, we introduce a colourful image to calculate the maximum gradient for different images. The gradient $G(i,j)$ at pixel (i,j) is calculated by [45]:

$$G(i,j) = \sqrt{(I(i,j) - I(i,j+1))^2 + (I(i,j) - I(i+1,j))^2} \quad (1)$$

The first row of Figure 2 shows a colourful image and corresponding channel images, as well as the greyscale image. Different images are divided into different regions with the same size. The regions with the maximum gradient among different images were painted grey, while the region with the maximum gradient among all regions was painted white. It can be seen that different regions with the maximum gradients are distributed in different channel images, not only in the greyscale image. Actually, the regions with the maximum gradients are distributed in channel images in most cases.

3 | THE PROPOSED METHOD

3.1 | The framework of DMLI

The framework of DMLI is illustrated in Figure 3. As the first step, a colourful image is changed to a greyscale image and the ROI is selected from the greyscale image through the first maximum local information strategy. The colourful image inside the ROI is selected for subsequent processing. Second, the colourful ROI is divided into three channel images, and the maximum local information is calculated from all different channel images to derive the final evaluation score.

3.2 | ROI extraction based on maximum gradient and local entropy

When an image is divided into several regions (or blocks), the local entropy of each region which is related to the variance of greyscale in the neighbourhood is different among regions. The entropy is higher for a heterogeneous region but lower for a homogeneous region [46]. Figure 4 shows local entropy distribution for different regions in an image. The regions with higher entropy are darker than the regions with lower entropy.

The regions with higher entropy would be more helpful for calculating IQA metric than the regions with lower entropy in edge information-based methods, because such regions represent the edge area of the image. Meanwhile, inspired by the maximum information-based methods [44, 45] which obtained superior performance, we also introduce the maximum gradient-based scheme presented in [45] to assist the ROI extraction. As a result, we propose the first maximum local information strategy, which combines the maximum gradient and local entropy to extract the ROI from a colourful image before calculating the evaluation result.

No-overlapped region division method is used in the original method [46], as illustrated in Figure 4. To avoid weakening the potential region with the highest entropy, the overlapped region division scheme is introduced in our method, as shown in Figure 5. A sliding window moves from top-left to bottom-right in an image.

After dividing an image into different regions with the sliding window, we calculate the maximum gradient via Equation (1) for each region.

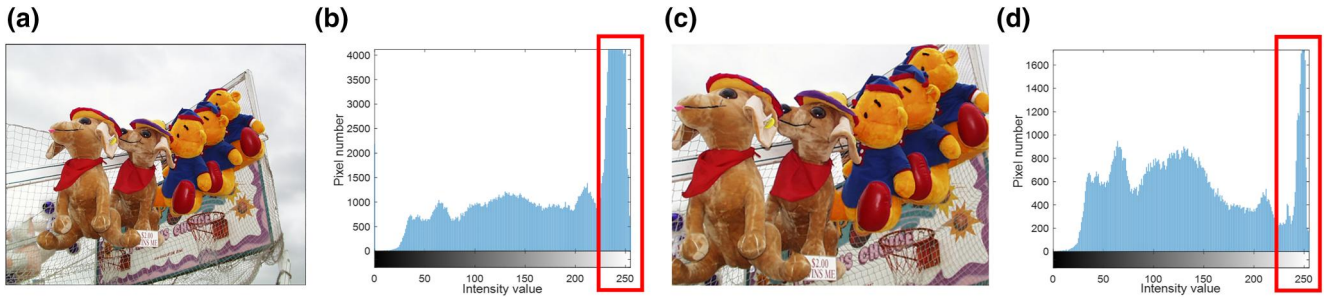

FIGURE 1 Images and corresponding histograms. (a) shows an original image from LIVE database [43] and (c) shows its corresponding extracted area in which smooth background was excluded, (b) and (d) show the histograms for greyscale image of (a) and (c), respectively

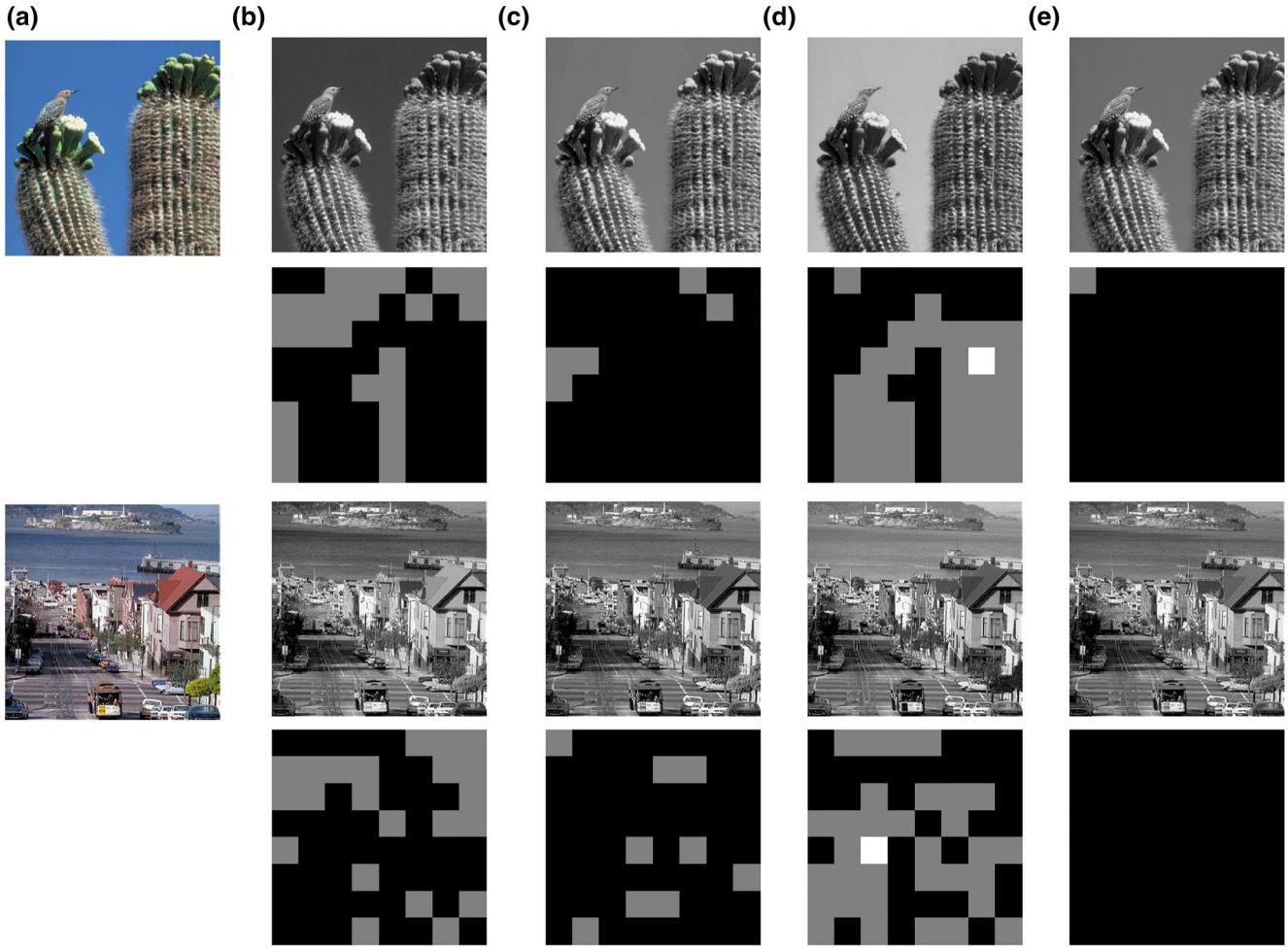

FIGURE 2 Different images with labels illustrated regions with the maximum gradients. (a) shows original colourful images; (b)–(e) show red channel images, green channel images, blue channel images, greyscale images and corresponding labels illustrated regions with the maximum gradients. The grey regions show the regions with the maximum gradients among different images. The white region shows the region with the maximum gradient among all regions

Then, the regions with the maximum gradient are selected for calculating local entropy, as illustrated below [40]:

$$E = -\sum_{l=0}^{L-1} P_l \log P_l \tag{2}$$

where L represents the maximum greyscale. P_l is the probability of greyscale l in the image given as follows:

$$P_l = \frac{n_l}{M \times N} \tag{3}$$

where n_l represents the number of pixels with greyscale l, and $M \times N$ represents the region size.

Finally, the region with the highest entropy is selected as the ROI. The size of the ROI is fixed beforehand, as described in Section 4.2.

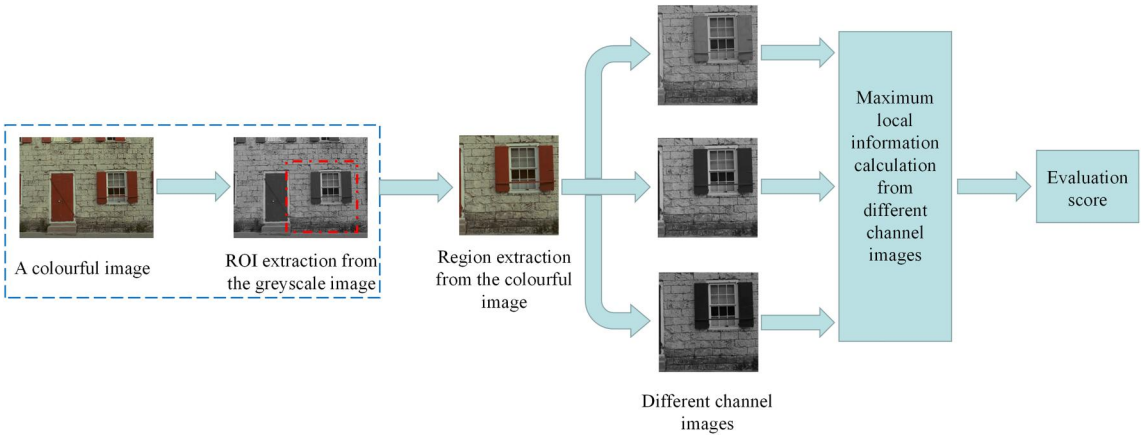

FIGURE 3 Flow-chart of the proposed Dual Maximum Local Information framework

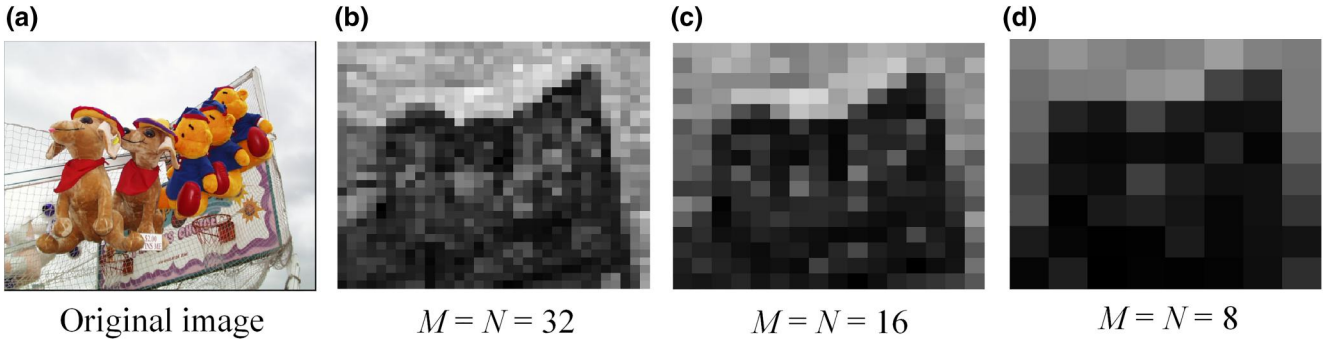

FIGURE 4 Local entropy of the greyscale image with different block numbers. *M* and *N* represent block number for each row and column when dividing the greyscale image

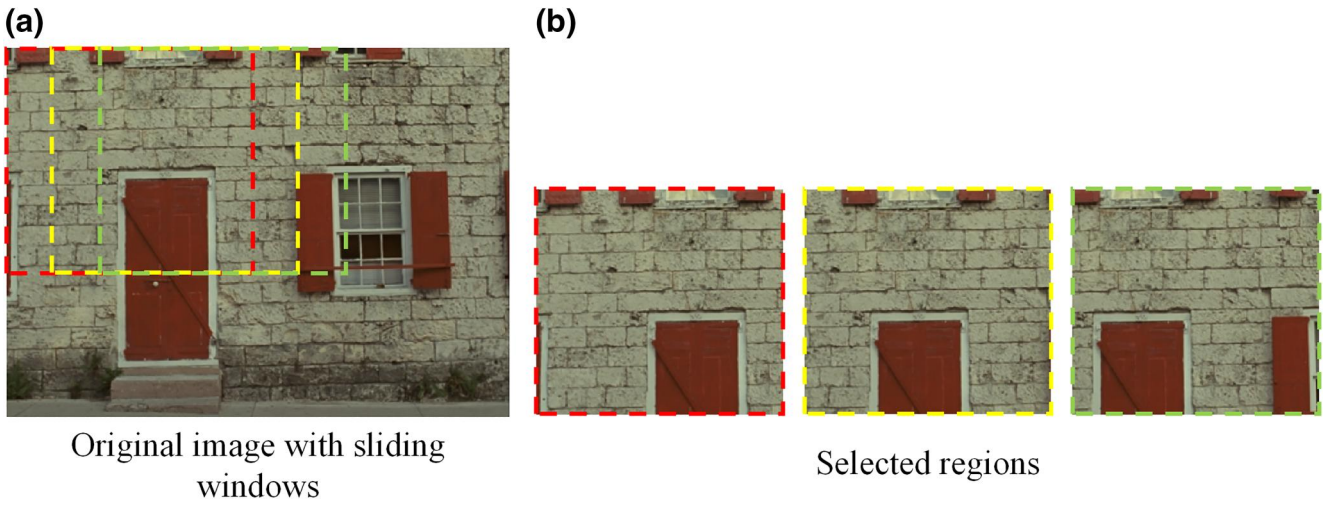

FIGURE 5 Overlapped region division method used in the proposed method

It is worth noting that since overlapped region division method is used in our method, there will be several neighbouring regions with the same maximum gradient. That is the reason why we introduce local entropy for ROI extraction after obtaining the regions with the maximum gradient. When there are more regions with the same entropy value, the first region in order will be chosen as the final ROI.

3.3 | Maximum gradient based on three channel images

For both MLV [44] and Zhan's method [45], the transformation from a colourful image into a greyscale image was the first step when calculating the metric. However, for a colourful image, three different channel images include much

more information than the greyscale image, which is described in Section 2.2. To take advantage of such information, we divide the ROI image into three channel images according to certain colour space. Then, three channel images are used for calculating both the maximum gradient and the variability of gradient as illustrated below:

$$MaxG = \max[G_{C1}(i,j), G_{C2}(i,j), G_{C3}(i,j)] \quad (4)$$

$$MinG = \min[G_{C1}(i,j), G_{C2}(i,j), G_{C3}(i,j)] \quad (5)$$

$$MeanG = \text{mean}[G_{C1}(i,j), G_{C2}(i,j), G_{C3}(i,j)] \quad (6)$$

$$VG = (MaxG - MinG)/MeanG \quad (7)$$

where G_{C1} (i, j), G_{C2} (i, j) and G_{C3} (i, j) represent gradient image for different channel images; $MaxG$, $MinG$ and $MeanG$ represent maximum, minimum and mean value among three different channel images, VG represents variability of gradient for three different channel images.

Finally, the evaluation score is obtained by

$$IQA = MaxG^{\alpha} \cdot VG^{1-\alpha} \quad (8)$$

where α equals 0.610 according to [45].

4 | PERFORMANCE EVALUATION

4.1 | Image databases and performance measures

To illustrate the subjective assessment consistent of DMLI, six widely used Gaussian blur related databases are introduced in performance evaluation, including LIVE [43], CSIQ [47], TID2008 [48], TID2013 [49], IVC [50] and VCL@FER [51]. The detailed information of these databases is illustrated in Table 1.

We compare the performance of DMLI with the existing NR-IQA methods in both spatial domain and spectral domain, including Re-blur [10], JNB [5], CPBD [6], S3 [16], LPC_SI [23], MLV [44], AR-based image sharpness metric (ARISM) [14], blind image bLur evaluation (BIBLE) [9], Zhan's Method [45], blind image SHARPness/blurriness assessment model (BISHARP) [22] and HVS-MaxPol [24]. All of these methods are blur-specific methods. The codes of these methods are publicly available. Four performance measures are used to evaluate the methods, including the following: (1) Pearson linear correlation coefficient (PLCC), (2) Spearman rank-order correlation coefficient (SROCC), (3) Mean-absolute error (MAE), and (4) Root-mean-square error (RMSE). The mathematical definition of these criteria can be found in [52]. Among these measures, higher PLCC, SROCC values and lower MAE, RMSE values indicate higher prediction accuracy, monotonicity, and consistency of a method. PLCC = SROCC = 1 and RMSE = MAE = 0 indicate a perfect match between the objective scores and the subjective scores. All experiments were performed on a Lenovo desktop computer with Intel® Core(TM) i7 CPU at 2.50 GHz and 2.59GHz with 8 GB RAM. The operating system is Windows 10 with 64-bit, and the experimental platform is MATLAB R2015a. Our pipeline is available at https://github.com/JamesC0321/DMLI.

4.2 | Impact of window size for ROI

To investigate the impact of window size on the performance of DMLI, we used different window sizes for ROI extraction according to the size of the original images. CSIQ and VCL@FER were used for illustration. For these two databases, window sizes range from 512 × 512 to 240 × 240, with step size of 8 × 8. For each window size, PLCC, SROCC, RMSE and MAE were calculated for comparison after obtaining the evaluation results. Table 2 lists the performance with different window sizes with step size of 32 × 32. It can be observed that the performance varies slightly among different window sizes, while the best performance is obtained when the window size is 416 × 416 for both databases. Therefore, the window size of 416 × 416 is adopted for CSIQ and VCL@FER. Similar experiments were carried out for LIVE, TID2008, TID2013 and IVC, and the window sizes are selected as 438 × 438, 280 × 280, 360 × 360 and 336 × 336, respectively. It is worth noting that we change the original RGB images in different databases into red channel image, green channel image and blue channel image in the experiments. To compare the computational complexity of the proposed method with different window sizes, we also compared the running times for different window sizes through different databases, as illustrated in Table 2. It can be found that when the window size decreases, running time increases. The reason is that when window size gets smaller, more regions are needed to be

TABLE 1 Detailed information of Gaussian blur images in different databases used in the experiments

Database	Image amount	Image size	Subjective quality	Value scales
LIVE	174	Different	DMOS	[0 100]
CSIQ	150	512 × 512	DMOS	[0 1]
TID2008	100	512 × 384	MOS	[0 9]
TID2013	125	512 × 384	MOS	[0 9]
IVC	20	512 × 512	MOS	[1 5]
VCL@FER	138	Different	MOS	[0 100]

calculated for the maximum gradient and local entropy to extract the ROI. It can also be observed that running time reaches the highest value when window size is 384 × 384. The reason is that when window size decreases, the running time for calculating a single region also decreases, so the total running time decreases. Figure 6 shows two images from CSIQ

TABLE 2 Comparison of performance and running time with different window sizes and measurements for two databases

Database (image size)	Window size	512 × 512	480 × 480	448 × 448	416 × 416	384 × 384	352 × 352
CSIQ (512 × 512)	PLCC	0.9742	0.9741	0.9744	**0.9749**	0.9741	0.9743
	SROCC	0.9597	0.9588	0.9589	**0.9595**	0.9586	0.9583
	RMSE	0.0646	0.0647	0.0644	**0.0638**	0.0648	0.0645
	MAE	0.0513	0.0516	0.0513	**0.0508**	0.0522	0.0517
	Time (sec)	0.0668	0.2706	0.6527	1.1535	1.5255	1.2081
Database (image size)	**Window size**	**512 × 512**	**480 × 480**	**448 × 448**	**416 × 416**	**384 × 384**	**352 × 352**
VCL@FER (different)	PLCC	0.9323	0.9334	0.9387	**0.9391**	0.9357	0.9349
	SROCC	0.9211	0.9223	0.9287	**0.9303**	0.9258	0.9253
	RMSE	8.8072	8.7377	8.3939	**8.3692**	8.5960	8.6452
	MAE	6.3439	6.2694	**6.0910**	6.1257	6.2701	6.4018
	Time (sec)	0.3528	1.4929	2.7174	3.9885	4.0047	3.0736

Note: The best result in each database is marked in boldface.

Abbreviations: MAE, mean-absolute error; PLCC, Pearson linear correlation coefficient; RMSE, root-mean-square error; SROCC, Spearman rank-order correlation coefficient.

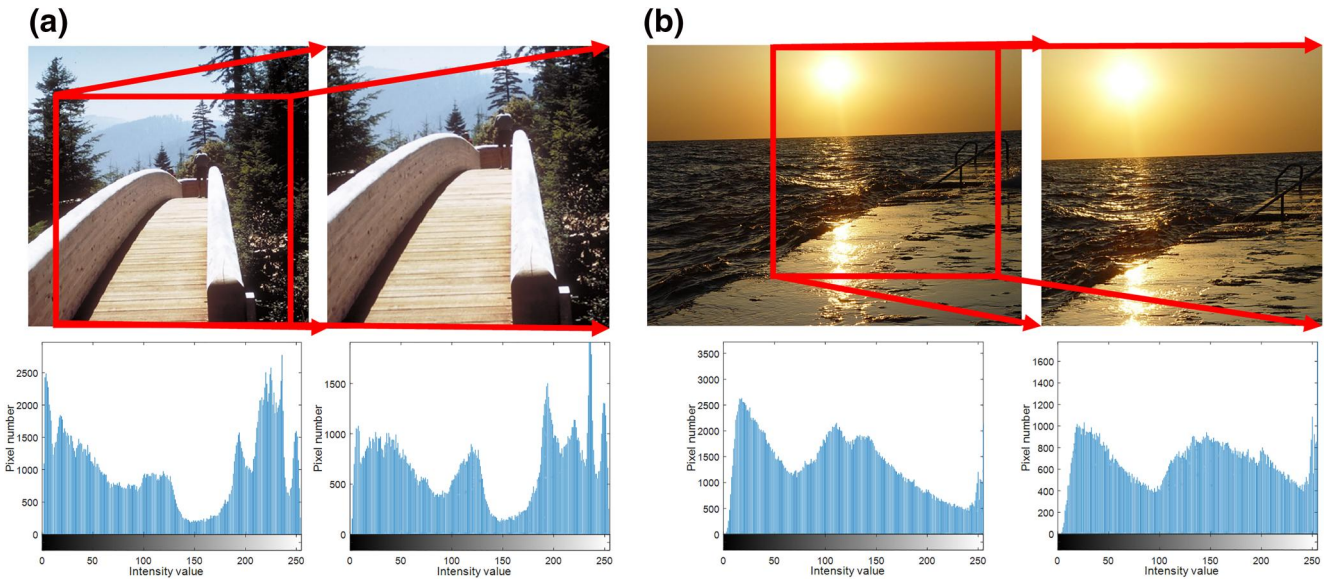

FIGURE 6 Original images from different databases and corresponding extraction results. (a) shows an image from the CSIQ and the extraction result, as well as the corresponding histograms, (b) shows an image from VCL@FER and the extraction result, as well as the corresponding histograms

TABLE 3 The performance comparison with different colour spaces and different measurements for two databases

Database	CSIQ				VCL@FER			
Measurement	RGB	HSV	LAB	YCbCr	RGB	HSV	LAB	YCbCr
PLCC	**0.9749**	0.6840	0.9549	0.9683	**0.9391**	0.7110	0.9082	0.9317
SROCC	**0.9595**	0.6899	0.9336	0.9510	**0.9303**	0.7056	0.9014	0.9165
RMSE	**0.0638**	0.2102	0.0851	0.0716	**8.3692**	17.1276	10.1937	8.8455
MAE	**0.0508**	0.1511	0.0680	0.0572	**6.1257**	13.7860	7.3635	6.5459

Note: The best result in each database is marked in boldface.

Abbreviations: MAE, mean-absolute error; PLCC, Pearson linear correlation coefficient; RMSE, root-mean-square error; SROCC, Spearman rank-order correlation coefficient.

TABLE 4 Comparison of different NR-IQA methods with different performance measurements for different IQA databases

Database	LIVE				CSIQ			
Method	**PLCC**	**SROCC**	**RMSE**	**MAE**	**PLCC**	**SROCC**	**RMSE**	**MAE**
Re-blur	0.9061	0.9195	9.2012	7.4079	0.8705	0.8461	0.1410	0.1126
JNB	0.8428	0.8423	11.7062	9.2405	0.7856	0.7624	0.1797	0.1224
CPBD	0.9128	0.9430	8.8820	6.8200	0.8740	0.8845	0.1396	0.1109
S3	0.9189	0.9634	8.5781	7.3352	0.8941	0.9058	0.1347	0.1095
LPC_SI	0.9066	0.9226	9.1772	7.2748	0.9225	0.9221	0.1109	0.0929
MLV	0.9589	0.9566	6.1708	4.8963	0.9488	0.9246	0.0905	0.0707
ARISM	0.9621	0.9679	5.9316	**4.5117**	0.9443	0.9254	0.0946	0.0764
BIBLE	**0.9627**	**0.9728**	**5.8834**	4.6052	0.9403	0.9130	0.0975	0.0774
Zhan's method	0.9602	0.9634	6.0776	4.6970	0.9666	0.9500	0.0734	0.0578
BISHARP	0.9515	0.9598	6.6936	5.2802	0.9416	0.9270	0.0967	0.0784
HVS-MaxPol	0.9569	0.9596	6.3176	5.0762	0.9381	0.9208	0.0994	0.0818
Proposed (whole image)	0.9568	0.9603	6.3231	4.7969	0.9742	**0.9597**	0.0646	0.0513
DMLI	0.9624	0.9660	5.9084	4.5218	**0.9749**	0.9595	**0.0638**	**0.0508**
Database	**TID2008**				**TID2013**			
Method	**PLCC**	**SROCC**	**RMSE**	**MAE**	**PLCC**	**SROCC**	**RMSE**	**MAE**
Re-blur	0.7838	0.7767	0.7288	0.5930	0.8091	0.7911	0.7333	0.6126
JNB	0.6611	0.6667	0.8805	0.6730	0.6946	0.6902	0.8978	0.6865
CPBD	0.8198	0.8412	0.6720	0.5243	0.8543	0.8518	0.6486	0.5263
S3	0.8505	0.8415	0.6174	0.4784	0.8790	0.8608	0.5950	0.4799
LPC_SI	0.8608	0.8959	0.5989	0.4780	0.8692	0.9191	0.6207	0.5073
MLV	0.8582	0.8546	0.6023	0.4681	0.8826	0.8786	0.5866	0.4604
ARISM	0.8427	0.8505	0.6317	0.4920	0.8945	0.8980	0.5580	0.4416
BIBLE	0.8929	0.8915	0.5284	0.4128	0.9048	0.8988	0.5313	0.4267
Zhan's method	0.9370	0.9419	0.4100	0.3209	0.9540	0.9605	0.3740	0.2877
BISHARP	0.8770	0.8797	0.5640	0.4386	0.8915	0.8959	0.5653	0.4488
HVS-MaxPol	0.8533	0.8507	0.6119	0.4843	0.8774	0.8746	0.5988	0.4838
Proposed (whole image)	0.9403	0.9435	0.3995	0.3108	0.9547	0.9611	0.3715	0.2846
DMLI	**0.9487**	**0.9531**	**0.3711**	**0.2868**	**0.9568**	**0.9630**	**0.3630**	**0.2837**
Database	**VCL@FER**				**IVC**			
Method	**PLCC**	**SROCC**	**RMSE**	**MAE**	**PLCC**	**SROCC**	**RMSE**	**MAE**
Re-blur	0.9059	0.8928	10.3134	8.4457	0.8772	0.8315	0.5481	0.4295
JNB	0.7486	0.7426	16.1491	12.6790	0.6909	0.6659	0.8255	0.6275
CPBD	0.8954	0.8630	10.8427	8.7715	0.8021	0.7690	0.6818	0.5304
S3	0.7244	0.5908	16.7924	13.3177	0.9261	0.8691	0.4307	0.3444
LPC_SI	0.9131	0.9127	9.9313	7.3540	0.9579	0.9533	0.3315	0.2621
MLV	0.7684	0.5270	15.5876	11.9913	0.9808	0.9767	0.2224	**0.1531**
ARISM	**0.9396**	0.9228	**8.3386**	6.7929	0.8534	0.7863	0.5952	0.4460
BIBLE	0.8889	0.8594	11.1583	8.1544	0.9785	0.9676	0.2354	0.1760
Zhan's method	0.9281	0.9150	9.0665	6.6972	0.9698	0.9752	0.2786	0.1917
BISHARP	0.5463	0.6185	20.4020	16.5704	0.9683	0.9684	0.2854	0.2143
HVS-MaxPol	0.5247	0.3471	20.7359	17.1875	0.9378	0.8879	0.3963	0.3438

TABLE 4 (Continued)

Database	VCL@FER				IVC			
Method	**PLCC**	**SROCC**	**RMSE**	**MAE**	**PLCC**	**SROCC**	**RMSE**	**MAE**
Proposed (whole image)	0.9323	0.9211	8.8072	6.3439	0.9681	0.9617	0.2862	0.2103
DMLI	0.9391	**0.9303**	8.3692	**6.1257**	**0.9859**	**0.9789**	**0.1910**	0.1624

Note: The best result is marked in boldface.

Abbreviations: ARISM, AR-based image sharpness metric; BIBLE, blind image bLur evaluation; BISHARP, blind image SHARPness/blurriness assessment model; CPBD, cumulative probability of blur detection; DMLI, Dual Maximum Local Information; JNB, Just Noticeable Blur; MAE, mean-absolute error; MLV, Maximum Local Variation; PLCC, Pearson linear correlation coefficient; RMSE, root-mean-square error; SROCC, Spearman rank-order correlation coefficient.

and VCL@FER, respectively, as well as the ROI extraction results and corresponding histograms. Most redundant regions are excluded after extraction.

4.3 | Impact of different colour spaces

For a colourful image, there are several different colour spaces, which provide more information about the image, including RGB, HSV, LAB, and YCbCr. We also introduce different colour spaces for comparisons in our experiments. CSIQ and VCL@FER were used for illustration. Table 3 lists the evaluation performance of different colour spaces for our method with the same size (416 × 416). It can be observed that RGB obtained the best performance among the four different colour spaces. We also conducted the same experiments for other databases. For TID2008, RGB also has the best performance, whereas for LIVE, TID2013 and IVC, YCbCr owns slightly better performance than that of RGB. As a result, YCbCr is selected for LIVE, TID2013 and IVC.

4.4 | Comparison with different databases

In this part, six image databases are used to evaluate the performance of different methods in Section 4.1. Table 4 summarises the performance comparison of the 12 methods on the six databases in terms of PLCC, SROCC, RMSE, and MAE. Overall, methods based on maximum information achieve better performance than the methods based on Sobel operator, which means maximum information is more important for evaluating blurriness of an image than choosing different gradient operators. The proposed method achieves the best results for most measurements in six databases. Specifically, DMLI achieves best results in CSIQ, TID2008, and TID2013 for all measurements. For other databases, DMLI achieves the best results for SROCC and MAE in VCL@FER, and the best results for PLCC, SROCC and RMSE for IVC. ARISM, MLV and BIBLE achieve the best results for other measurements. Compared with Zhan's method, DMLI achieves better performance for all measurements, which infers that the proposed framework can enhance the performance of maximum information-based method. We also used the proposed method without the ROI extraction for comparison. Most results obtained by DMLI are better than the proposed method without the ROI extraction, which demonstrates the benefit of the ROI extraction strategy.

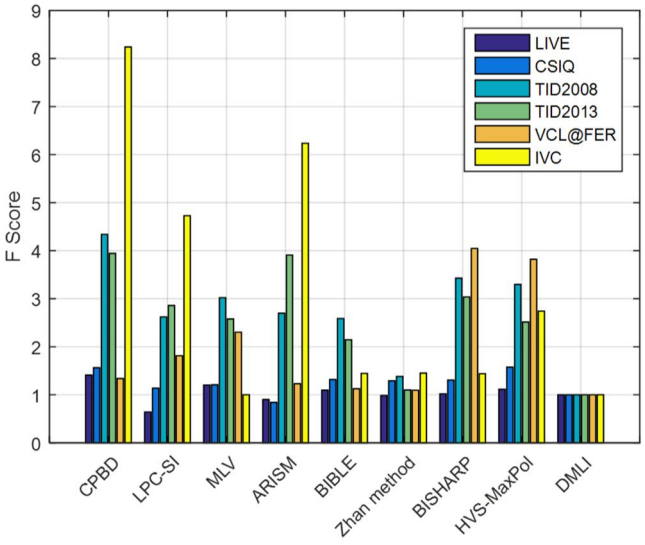

FIGURE 7 *F*-test results of eight leading no-reference image quality assessment methods against the proposed method on six databases

F-test [43] is leveraged to assess whether the proposed method has better (or worse) evaluation results than another method. Value of $F > F_{critical}$ (or $F < 1/F_{critical}$) indicates that the proposed method is statistically better (or worse) than another method at a certain confidence level. To further quantify the statistical significance, our method compared with some leading methods is listed in Table 4, *F*-test is introduced. Eight typical methods are selected for comparisons, as illustrated in Figure 7. It can be observed that our method produces either lower or comparable prediction errors among the most leading methods. Table 5 presents the statistical significance results at a confidence level of 0.95. Our method performs better than 56.3% of the alternative methods.

Figure 8 shows the scatter plots between the objective scores and the subjective scores on the four classical databases. These methods own better performance than the other existing methods in the previous six databases, as listed in Table 4. The method with ideal performance should produce scatter points close to the diagonal line. Our method produces good

TABLE 5 *F*-test of NR-IQA methods of six databases

Database	Criterion	CPBD	LPC_SI	MLV	ARISM	BIBLE	Zhan's method	BISHARP	HVS-MaxPol	DMLI
LIVE	$F_{critical}$ = 1.2841	**1.4095**	0.6416	1.2020	0.9013	1.0965	0.9864	1.0201	1.1172	1
CSIQ	$F_{critical}$ = 1.3093	**1.5645**	1.1379	1.2082	0.8418	**1.3161**	1.2905	1.3076	**1.5748**	1
TID2008	$F_{critical}$ = 1.3917	**4.3383**	**2.6207**	**3.0208**	**2.6980**	**2.5876**	1.3823	**3.4284**	**3.2976**	1
TID2013	$F_{critical}$ = 1.3436	**3.9438**	**2.8589**	**2.5776**	**3.9080**	**2.1465**	1.0991	**3.0362**	**2.5138**	1
VCL@FER	$F_{critical}$ = 1.3245	**1.3389**	**1.8126**	**2.3028**	1.2310	1.1257	1.0935	**4.0470**	**3.8209**	1
IVC	$F_{critical}$ = 2.1245	**8.2411**	**4.7281**	1	**6.2360**	1.4453	1.4516	1.4381	**2.7409**	1

Note: The results which are larger than criterion are marked in boldface.

Abbreviations: ARISM, AR-based image sharpness metric; BIBLE, blind image bLur evaluation; DMLI, Dual Maximum Local Information; MLV, Maximum Local Variation; NR-IQA, no-reference image quality assessment.

fittings for all databases, as illustrated in Figure 8. For CSIQ, TID2008, and TID2013, our method produces the best fittings. LIVE, ARISM, BIBLE, Zhan's method and our method produce similar results, which is consistent with the evaluation results shown in Table 4.

4.5 | Comparison with different images

We also tested DMLI with some blurred images from different databases. Four images with decreasing blurriness from CSIQ and corresponding evaluation scores are shown in Figure 9. For comparison, we also provided the evaluation results of twelve NR-IQA methods. It can be found that DMLI can obtain evaluation results which are consistent with the DMOS values. Most methods produce the monotonically decreasing/increasing blur scores which are consistent with DMOS. ARISM produces incorrect results between image 124 and image 108, as the evaluation score of image 124 is higher than that of image 108.

Then, we evaluated different methods on one subject with different blurriness from the LIVE, as shown in Figure 10. Images are presented from top-left to bottom-right according to decreasing extents of blur. Compared with the clear image, images with blurriness miss detailed information, especially in the edge area. For example, abundant information is around the eyes of parrots in image 154, but that information disappears in image 69. Most methods produce reasonable evaluation scores monotonically including DMLI. Re-blur and CPBD generate incorrect evaluation scores between image 69 and image 105. We also draw curves for 10 methods except Re-blur and CPBD, as shown in Figure 11. Curve of DMOS is also presented for comparison. It should be noted that DMOS for LIVE is range from 100 to zero, which represents blur to clarity. To be consistent with the scores produced by different methods, we use 100 minus the original DMOS to obtain the curve. MLV, Zhan's method, BISHARP, BIBLE, HSV-MaxPol and DMLI have similar curves compared with DMOS.

4.6 | Running time comparison

We also compared the mean running time of all NR-IQA methods which are implemented on 174 images from LIVE. The results are summarised in Table 6. The mean time spent by S3 and ARISM are much longer than that of the other methods. Most methods take less than 1 s to process one image. Some of them even require less than 100 ms for each image. For DMLI, when we implemented it without the ROI extraction step, the running time is only 0.047 s, which means that most of the running time for DMLI is spent on the ROI extraction step. Among these methods, Zhan's method has the lowest running time.

4.7 | Comparison with learning-based methods

In previous experiments, we concentrated on the NR-IQA methods without training. In this section, we introduced learning-based methods for comparison, as shown in Table 7. Among these methods, BIQI [28], BLIINDS-II [26], BRISQUE [27], SSEQ [53], Cai's method [30] and Liu's method [31] are based on SVM, Kang's CNN [32], Yu's CNN [54], MEON [34], SGDNet [36], NSSADNN [35] and MSFF [37] are based on deep learning. NIQE [55] and SPARISH [56] belong to other learning-based methods. BIQI [28], BLIINDS-II [26], BRISQUE [27], SSEQ [53], NIQE [55], Kang's CNN [32], MEON [34], SGDNet [36], NSSADNN [35] and MSFF [37] were proposed for general purpose, while the rest of the methods are blur-specific. Most of the codes and training models of previous methods are publicly available, but considering that the training environments and settings vary among different learning-based methods, the results of those methods were obtained directly from the corresponding reference papers [30, 31, 35, 37, 53, 57, 58]. We introduced PLCC and SROCC as measurements. Four classical databases are used for comparison. As shown in Table 7, DMLI still achieves competitive results compared with learning-based methods. Specifically, DMLI achieves the best value for PLCC and SROCC in CSIQ and TID2008. All the results obtained by DMLI are in the top three for PLCC and SROCC in CSIQ, TID2008 and TID2013.

5 | DISCUSSIONS AND CONCLUSION

Blur is an important image degradation among different image distortion types. An efficient no-reference blurred IQA

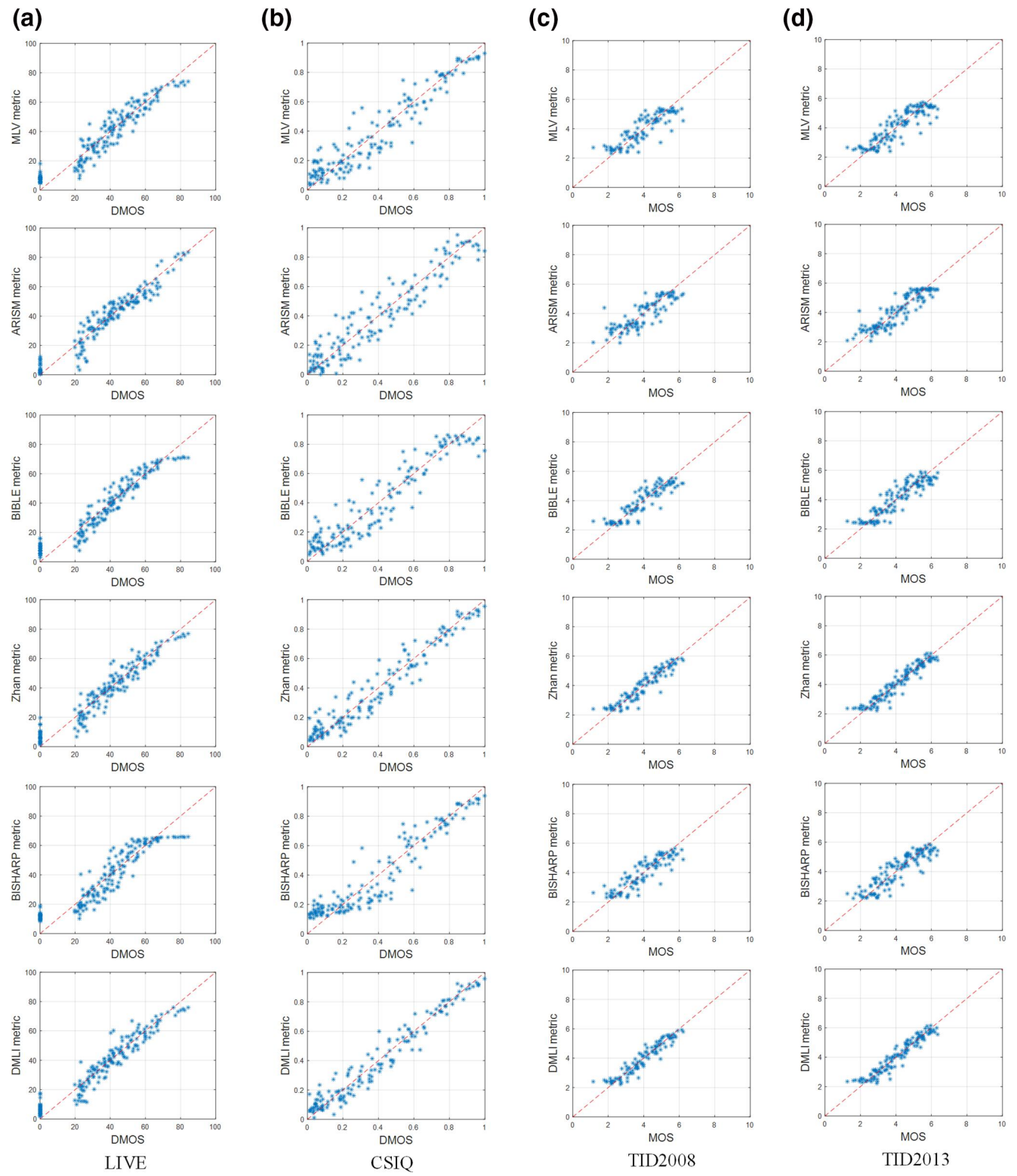

FIGURE 8 Scatter plot of DMOS/MOS with different no-reference image quality assessment methods for four classical databases

method is vital in measuring the extent of image blur. In this paper, we proposed an NR-IQA method based on DMLI. Inspired by image processing-based auto-focussing theory that the focussing region in an image could provide more important information than other regions, we proposed the first maximum local information, which combines the maximum gradient and local entropy to extract the ROI in a colourful image for subsequent processing. Then, based on the maximum gradient from different channel images, the second maximum local information was proposed to calculate the final

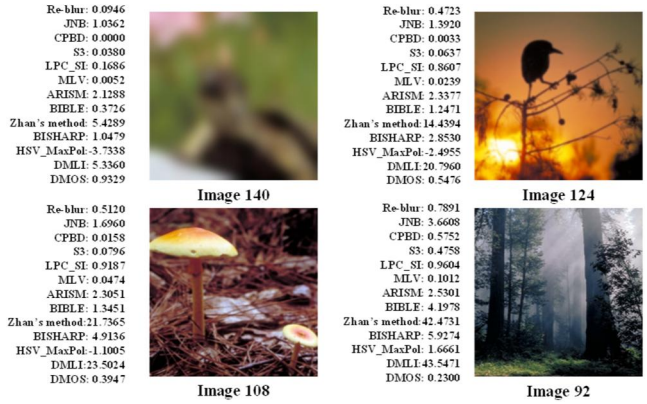

FIGURE 9 Four images with decreasing extents of blur from CSIQ and corresponding evaluation scores from different methods and DMOS

evaluation score. Through evaluation results, it can be concluded that the ROI extraction can enhance the performance of DMLI, and different channel images bring more information than the greyscale image.

The framework of DMLI is also helpful for other maximum information-based methods to improve the performance. We combined our framework with MLV, as illustrated in Table 8. With the proposed framework, the performance of MLV improves for four classical databases.

The ROI strategy used in the proposed method can be affected by region selection strategy in auto-focussing method. For example, some images may be captured with multiple focussing regions, resulting in diverse contents with overall high focus, while others may be captured with only one special region. For the proposed method, we only

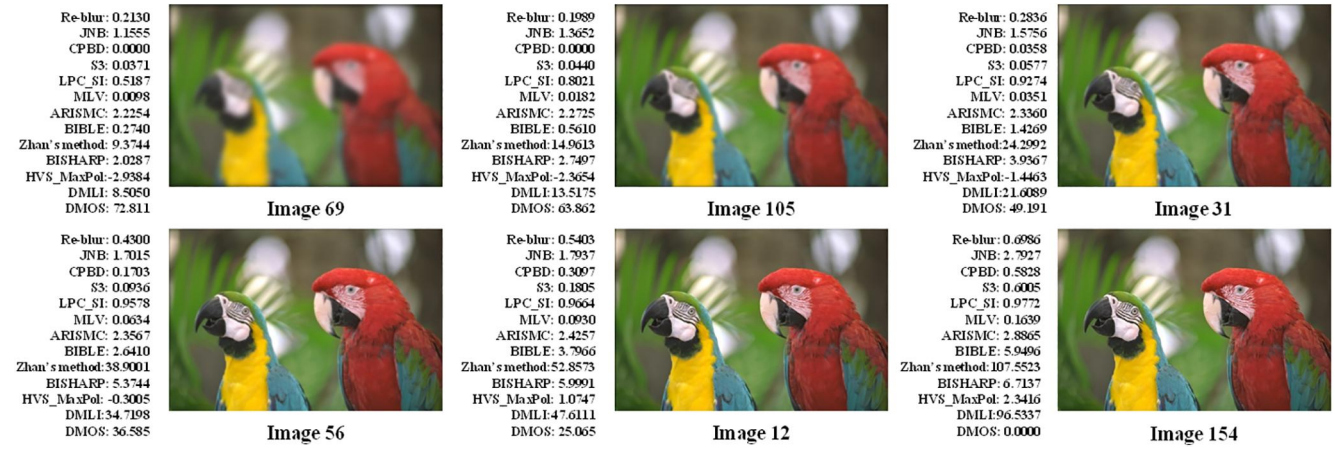

FIGURE 10 Six images with decreasing extents of blur from LIVE and corresponding evaluation scores via different methods and DMOS

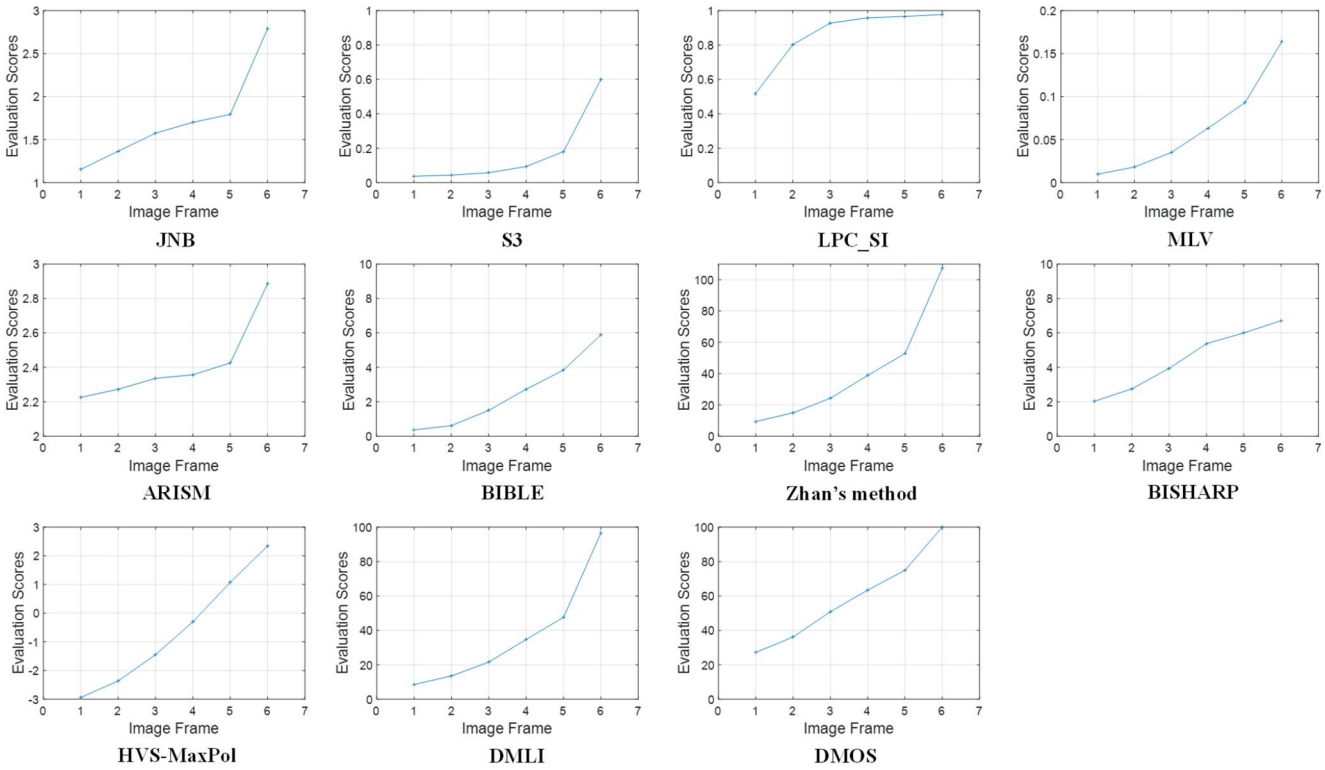

FIGURE 11 Different curves according to evaluation scores via different methods for images from LIVE and DMOS

TABLE 6 Mean running time of different methods for generating evaluation results for each image in LIVE

Method	Re-blur	JBN	CPBD	S3	LPC_SI	MLV
Time (sec)	0.070	0.564	0.735	44.672	1.712	0.120
Method	**ARISM**	**BIBLE**	**Zhan's method**	**BISHARP**	**HVS-MaxPol**	**DMLI**
Time (sec)	37.395	4.416	0.017	0.132	0.097	2.195

Abbreviations: ARISM, AR-based image sharpness metric; BIBLE, blind image bLur evaluation; BISHARP, blind image SHARPness/blurriness assessment model; DMLI, Dual Maximum Local Information; JNB, Just Noticeable Blur; MLV, Maximum Local Variation.

TABLE 7 DMLI versus learning-based methods with different performance measurements for different databases

Database		LIVE		CSIQ		TID2008		TID2013	
Method	Year	PLCC	SROCC	PLCC	SROCC	PLCC	SROCC	PLCC	SROCC
BIQI	2010	0.920	0.914	0.846	0.773	0.794	0.799	0.825	0.815
BLIINDS-II	2011	0.939	0.931	0.886	0.892	0.842	0.859	0.857	0.862
BRISQUE	2012	0.951	0.943	0.921	0.907	0.866	0.865	0.862	0.861
NIQE	2013	0.939	0.930	0.918	0.891	0.832	0.823	0.816	0.807
Kang's CNN	2014	0.963	**0.983**	0.774	0.781	0.880	0.850	0.931	0.922
SSEQ	2014	0.961	0.948	0.871	0.870	0.858	0.852	0.863	0.862
SPARISH	2016	0.960	0.960	0.939	0.914	0.896	0.896	0.902	0.894
Yu's CNN	2017	**0.973**	0.965	0.942	**0.925**	**0.937**	**0.919**	0.922	0.914
MEON	2018	0.948	0.940	0.916	0.905	-	-	0.891	0.880
SGDNet	2019	0.946	0.939	0.866	0.860	-	-	0.928	0.914
NSSADNN	2019	**0.984**	**0.986**	0.927	0.893	-	-	0.910	0.844
Liu	2020	**0.980**	**0.973**	**0.955**	**0.936**	-	-	**0.972**	**0.964**
Cai	2020	0.958	0.955	**0.952**	0.923	-	-	**0.957**	**0.941**
MSFF	2020	0.954	0.962	-	-	**0.925**	**0.928**	0.921	0.928
DMLI		0.962	0.966	**0.975**	**0.960**	**0.949**	**0.953**	**0.957**	**0.963**

Note: The top three results are marked in boldface.

Abbreviations: DMLI, Dual Maximum Local Information; PLCC, Pearson linear correlation coefficient; SROCC, Spearman rank-order correlation coefficient.

TABLE 8 The performance comparison of MLV without/with the proposed framework

Database	LIVE				CSIQ			
Measurement	PLCC	SROCC	RMSE	MAE	PLCC	SROCC	RMSE	MAE
Without	0.9589	0.9566	6.1708	4.8963	0.9488	0.9246	0.0905	0.0707
With	**0.9639**	**0.9611**	**5.7903**	**4.6509**	**0.9638**	**0.9466**	**0.0764**	**0.0602**
Database	**TID2008**				**TID2013**			
Measurement	**PLCC**	**SROCC**	**RMSE**	**MAE**	**PLCC**	**SROCC**	**RMSE**	**MAE**
Without	0.8582	0.8546	0.6023	0.4681	0.8826	0.8786	0.5866	0.4604
With	**0.8675**	**0.8724**	**0.5838**	**0.4457**	**0.8955**	**0.8959**	**0.5553**	**0.4407**

Note: The better result is marked in boldface.

Abbreviations: MAE, mean-absolute error; MLV, Maximum Local Variation; PLCC, Pearson linear correlation coefficient; RMSEA, root-mean-square error; SROCC, Spearman rank-order correlation coefficient.

choose one region as the final ROI, which is not suitable for images with multiple focussing regions. Besides, we introduced entropy calculation for ROI extraction in the proposed method, which may be affected by noise. We also introduced both Gaussian noise and impulse noise (salt and pepper) to show the effect of noise on ROI extraction. Specifically, we added Gaussian noise and impulse noise separately to images in CSIQ and VCL@FER, and compared

Database	CSIQ		VCL@FER	
Noise type	Gaussian noise	Impulse noise	Gaussian noise	Impulse noise
Consistent percentage	39.33%	56.67%	23.19%	26.81%

TABLE 9 Region of interest (ROI) selection consistency percentage for image without/with noise. Consistency percentage is calculated by the number of images with the same ROI without/with noise to total image number in different databases

the ROI selection results for images without/with noise. As illustrated in Table 9, when noise is added, some selected ROIs are different between images without/with noise. In future work, we will try the ROI strategy with multiple regions, and make balance between region size and region number. We will also explore some other ROI selection methods that can be immune to different types of noise.

To evaluate the performance of the proposed method, we tested DMLI and several existing training-free methods on LIVE, CSIQ, TID2008, TID2013, VCL@FER and IVC databases. DMLI has better performance for most measurements. We also compared DMLI with the state-of-the-art learning-based methods, and experimental results show that DMLI can still achieve competitive results.

ACKNOWLEDGEMENTS

This work was partially supported by the Natural Science Foundation of Fujian Province [grant number: 2018J01637], Open Fund Project of Fujian Provincial Key Laboratory of Information Processing and Intelligent Control (Minjiang University) [grant number: MJUKF-IPIC202110] and the Natural Science Foundation of Shanghai [grant number: 19ZR1407200]. We thank Zhenghan Fang for checking grammar and spelling.

CONFLICT OF INTEREST

The authors declare that they have no conflict of interest in relation to the work in this article.

ORCID

Jian Chen https://orcid.org/0000-0003-0799-2455

REFERENCES

1. Li, L., et al.: No-reference quality assessment of deblurred images based on natural scene statistics. IEEE Access. 5, 2163–2171 (2017)
2. Chandler, D.M.: Seven challenges in image quality assessment: past, present, and future research, ISRN Signal Processing, 2013, 1–53 (2013)
3. Wang, Z.: Objective image quality assessment: facing the real-world challenges. In: IS&T International Symposium on Electronic Imaging, pp. 1–6 (2016)
4. Marziliano, P., et al.: Perceptual blur and ringing metrics: application to JPEG2000. Signal Process. Image Commun. 19(2), 163–172 (2004)
5. Ferzli, R., Karam, L.J.: A no-reference objective image sharpness metric based on the notion of just noticeable blur (JNB). IEEE Trans. Image Process. 18(4), 717–728 (2009)
6. Narvekar, N.D., Karam, L.J.: A no-reference image blur metric based on the cumulative probability of blur detection (CPBD). IEEE Trans. Image Process. 20(9), 2678–2683 (2011)
7. Feichtenhofer, C., Fassold, H., Schallauer, P.: A perceptual image sharpness metric based on local edge gradient analysis. IEEE Signal Process. Lett. 20(4), 379–382 (2013)
8. Chen, Y., et al.: Blind quality assessment for cartoon images. IEEE Trans. Circ. Syst. Video Technol. 30(9), 3282–3288 (2020)
9. Li, L., et al.: No-reference image blur assessment based on discrete orthogonal moments. IEEE Trans. Cybern. 46(1), 39–50 (2016)
10. Crete, F., et al.: The blur effect: perception and estimation with a new no-reference perceptual blur metric. In: Proceedings of SPIE on the International Society for Optical Engineering, pp. 64920I–64920I-11 (2007)
11. Bong, D.B.L., Khoo, B.E.: An efficient and training-free blind image blur assessment in the spatial domain. IEICE Trans. Info. Syst. E97.D(7), 1864–1871 (2014)
12. Zhang, H., et al.: No-reference blurred image quality assessment by structural similarity index. Appl Sci. 8(10), 2003 (2018)
13. Wang, Z., et al.: Image quality assessment: from error visibility to structural similarity. IEEE Trans. Image Process. 13(4), 600–612 (2004)
14. Gu, K., et al.: No-reference image sharpness assessment in autoregressive parameter space. IEEE Trans. Image Process. 24(10), 3218–3231 (2015)
15. Zhai, G., et al.: A psychovisual quality metric in free-energy principle. IEEE Trans. Image Process. 21(1), 41–52 (2012)
16. Vu, C.T., Phan, T.D., Chandler, D.M.: S3: a spectral and spatial measure of local perceived sharpness in natural images. IEEE Trans. Image Process. 21(3), 934–945 (2012)
17. Caviedes, J., Gurbuz, S.: No-reference sharpness metric based on local edge kurtosis. In: Proceedings on International Conference on Image Processing, pp. 53–56 (2002)
18. Zhang, S.Q., et al.: No-reference image blur assessment based on SIFT and DCT. J. Inf. Hiding Multimedia Signal Process. 9(1), 219–231 (2018)
19. Lowe, D.G.: Object recognition from local scale-invariant features. In: Proceedings of the seventh IEEE International Conference on Computer Vision, pp. 1150–1157 (1999)
20. Vu, P.V., Chandler, D.M.: A fast wavelet-based algorithm for global and local image sharpness estimation. IEEE Signal Process. Lett. 19(7), 423–426. (2012)
21. Ciancio, A., et al.: Objective no-reference image blur metric based on local phase coherence. Electron. Lett. 45(23), 1162–1163 (2009)
22. Gvozden, G., Grgic, S., Grgic, M.: Blind image sharpness assessment based on local contrast map statistics. J. Vis. Commun. Image Represent. 50, 145–158 (2018)
23. Hassen, R., Wang, Z., Salama, M.M.A.: Image sharpness assessment based on local phase coherence. IEEE Trans. Image Process. 22(7), 2798–2810 (2013)
24. Hosseini, M., Zhang, Y., Plataniotis, K.: Encoding visual sensitivity by MaxPol convolution filters for image sharpness assessment. IEEE Trans. Image Process. 28(9), 4510–4525 (2019)
25. Saad, M.A., Bovik, A.C., Charrier, C.: A DCT statistics-based blind image quality index. IEEE Signal Process. Lett. 17(6), 583–586 (2010)
26. Saad, M.A., Bovik, A.C., Charrier, C.: DCT statistics model-based blind image quality assessment. In: IEEE International Conference on Image Processing, pp. 3093–3096 (2011)
27. Mittal, A., Moorthy, A.K., Bovik, A.C.: No-reference image quality assessment in the spatial domain. IEEE Trans Image Process. 21(12), 4695–4708 (2012)
28. Moorthy, A.K., Bovik, A.C.: A two-step framework for constructing blind image quality indices. IEEE Signal Process. Lett. 17(5), 513–516 (2010)
29. Moorthy, A.K., Bovik, A.C.: Blind image quality assessment: from natural scene statistics to perceptual quality. IEEE Trans. Image Process. 20(12), 3350–3364 (2011)
30. Cai, H., et al.: No-reference image sharpness assessment based on discrepancy measures of structural degradation. J. Vis. Commun Image Represent. 71, 102861 (2020)
31. Liu, L., et al.: Blind image blur metric based on orientation-aware local patterns. Signal Process Image Commun. 80, 115654 (2020)

32. Kang, L., et al.: Convolutional neural networks for no-reference image quality assessment. In: IEEE Conference on Computer Vision and Pattern Recognition, pp. 1733–1740 (2014)
33. Bianco, S., et al.: On the use of deep learning for blind image quality assessment. Signal Image Vid. Process. 12(2), 355–362 (2018)
34. Ma, K., et al.: End-to-end blind image quality assessment using deep neural networks. IEEE Trans. Image Process. 27(3), 1202–1213 (2018)
35. Yan, B., Bare, B., Tan, W.: Naturalness-aware deep no-reference image quality assessment. IEEE Trans. Multimed. 21(10), 2603–2615 (2019)
36. Yang, S., et al.: SGDNet: an end-to-end saliency-guided deep neural network for no-reference image quality assessment. In: Proceedings of the 27th ACM International Conference on Multimedia, pp. 1383–1391 (2019)
37. He, S., Liu, Z.: Image quality assessment based on adaptive multiple Skyline query. Signal Process. Image Commun. 80, 115676 (2020)
38. Kim, Y., et al.: A video camera system with enhanced zoom tracking and auto white balance. IEEE Trans. Consum. Electron. 48(3), 428–434 (2002)
39. Wang, Y., Jiang, W., Zheng, Y.: Dynamic autofocussing region selection based on improved PSO. In: 2010 3rd IEEE International Congress on Image and Signal Processing, pp. 2760–2764 (2010)
40. Jeon, J., et al.: Fully digital auto-focussing system with automatic focussing region selection and point spread function estimation. IEEE Trans. Consum. Electron. 56(3), 1204–1210 (2010)
41. Liang, M., Wu, Z., Chen, T.: Auto-focussing adjustment of theodolites by largest the gradient method. Opt Precis Eng. 17(12), 3016–3021 (2009)
42. Lee, S.Y., et al.: Enhanced autofocus algorithm using robust focus measure and fuzzy reasoning. IEEE Trans. Circ. Syst. Video Technol. 18(9), 1237–1246 (2008)
43. Sheikh, H.R., Sabir, M.F., Bovik, A.C.: A statistical evaluation of recent full reference image quality assessment algorithms. IEEE Trans Image Process. 15(11), 3440–3451 (2006)
44. Bahrami, K., Kot, A.C.: A fast approach for no-reference image sharpness assessment based on maximum local variation. IEEE Signal Process. Lett. 21(6), 751–755 (2014)
45. Zhan, Y., Zhang, R.: No-reference image sharpness assessment based on maximum gradient and variability of gradients. IEEE Trans. Multimed. 20(7), 1796–1808 (2018)
46. Yan, C., Nong, S., Zhang, T.: Local entropy-based transition region extraction and thresholding. Pattern Recogn Lett. 24(16), 2935–2941 (2003)
47. Larson, E.C., Chandler, D.M.: Most apparent distortion: full-reference image quality assessment and the role of strategy. J. Electron. Imag. 19(1), 1–21 (2010)
48. Ponomarenko, N., et al.: TID2008 - a database for evaluation of Full-Reference visual quality assessment metrics. Adv. Modern Radioelectron. 10, 30–45 (2009)
49. Ponomarenko, N., et al.: Image database TID2013: peculiarities, results and perspectives. Signal Process. Image Commun. 30, 57–77 (2015)
50. Le Callet, P., Autrusseau, F.: Subjective quality assessment IRCCyN/IVC database (2005)
51. Zari, A.E., et al.: VCL@FER image quality assessment database. Automatika. 53(4), 344–354 (2012)
52. Wang, Z., Li, Q.: Information content weighting for perceptual image quality assessment. IEEE Trans. Image Process. 20(5), 1185–1198 (2011)
53. Liu, L., et al.: No-reference image quality assessment based on spatial and spectral entropies. Signal Process. Image Commun. 29(8), 856–863 (2014)
54. Yu, N., et al.: A shallow convolutional neural network for blind image sharpness assessment. PloS One. 12, e176632 (2017)
55. Mittal, A., Soundararajan, R., Bovik, A.C.: Making a completely blind image quality analyser. IEEE Signal Process. Lett. 20(3), 209–212 (2013)
56. Li, L., et al.: Image sharpness assessment by sparse representation. IEEE Trans. Multimed. 18(6), 1085–1097 (2016)
57. Li, L., et al.: No-reference and robust image sharpness evaluation based on multiscale spatial and spectral features. IEEE Trans. Multimed. 19(5), 1030–1040 (2017)
58. Zhang, Y., et al.: No-reference image sharpness assessment based on rank learning. In: IEEE International Conference on Image Processing, pp. 2359–2363 (2019)

How to cite this article: Chen, J., Li, S., Lin, L.: A no-reference blurred colourful image quality assessment method based on dual maximum local information. IET Signal Process. 15(9), 597–611 (2021). https://doi.org/10.1049/sil2.12064